

ElasticRec: A Microservice-based Model Serving Architecture Enabling Elastic Resource Scaling for Recommendation Models

Yujeong Choi
School of Electrical Engineering
KAIST
yjchoi0606@kaist.ac.kr

Jiin Kim
School of Electrical Engineering
KAIST
jiin.kim@kaist.ac.kr

Minsoo Rhu
School of Electrical Engineering
KAIST
mrhu@kaist.ac.kr

Abstract—With the increasing popularity of recommendation systems (RecSys), the demand for compute resources in datacenters has surged. However, the model-wise resource allocation employed in current RecSys model serving architectures falls short in effectively utilizing resources, leading to sub-optimal total cost of ownership. We propose ElasticRec, a model serving architecture for RecSys providing resource elasticity and high memory efficiency. ElasticRec is based on a microservice-based software architecture for fine-grained resource allocation, tailored to the heterogeneous resource demands of RecSys. Additionally, ElasticRec achieves high memory efficiency via our utility-based resource allocation. Overall, ElasticRec achieves an average $3.3\times$ reduction in memory allocation size and $8.1\times$ increase in memory utility, resulting in an average $1.6\times$ reduction in deployment cost compared to state-of-the-art RecSys inference serving system.

Index Terms—Machine learning, recommendation model, resource management, resource scaling, microservice, model deployment

I. INTRODUCTION

Deep neural network (DNN) based recommendation system (RecSys) accounts for a significant portion of machine learning (ML) inference cycles in modern datacenters (75% in Meta [20], 25% in Google [24]). These latency-critical ML services operate with stringent service level agreement (SLA) goals on tail latency, so maximizing latency-bounded throughput (i.e., number of service queries processed per second that meets SLA, aka QPS) becomes critical.

To serve billions of service queries around the world, datacenters replicate a large fleet of inference servers, each server replica provisioned with its own copy of the entire model parameters [18], [20], [28], [46]. Such baseline “model-wise” resource allocation enables each server replica to independently service user queries, which helps utilize query-level parallelism across the fleet and improve QPS. However, a critical limitation of model-wise resource allocation is that the way resources are allocated does not consider how well it is actually utilized, leading to significant waste in resources. This work identifies two key reasons behind the baseline’s sub-optimal resource allocation:

- 1) **Heterogeneous resource demands of sparse and dense layers in RecSys.** Modern RecSys combines sparse embedding layers with dense DNN layers, each layer

exhibiting notable differences in their compute and memory characteristics. Consequently, the QPS of a dense DNN layer and sparse embedding layer becomes uneven (i.e., one layer type typically shows much lower QPS than the other layer type), rendering the low-performance layer to bottleneck the overall QPS (Section III-A). To maximize end-to-end model-wise throughput, an optimal resource allocation would have *more compute resources provisioned just to the bottlenecked layer*. Unfortunately, the baseline model-wise resource allocation treats the entire RecSys model as one monolithic unit for allocating resources. As such, it is challenging to selectively provision more resources to only a subset of model layer(s), failing to satisfy the unique resource demands of each layer independently.

- 2) **Sparse embedding table accesses and its skewed access distribution.** The embedding tables employed in sparse embedding layers are memory capacity limited, amounting to several tens of GBs. Access patterns to these tables generally exhibit a power-law distribution where a small subset of (hot) table entries receive very high access frequency while the remaining (cold) entries receive only a small number of accesses. Because the baseline mechanism allocates resources in a coarse-grained, model-wise fashion, *each server replica must allocate the entire embedding tables in memory without accounting for the individual embedding’s actual “utility”*. As such, the baseline model-wise resource allocation suffers from significant memory waste and limits the total number of server replicas that can be instantiated across the datacenter fleet, deteriorating fleet-wide QPS.

To this end, we propose ElasticRec, a RecSys model serving architecture providing resource elasticity and high memory efficiency. The unique aspects of ElasticRec are twofold. First, our proposed system employs a *microservice-based* inference server for high resource elasticity. Second, ElasticRec achieves high memory efficiency via our *utility-based* resource allocation policy.

- **Microservice software architecture for RecSys.** ElasticRec employs the microservice [44] programming model as the core mechanism to enable fine-grained resource allocation that meets the heterogeneous resource demands of RecSys. The benefit of microservices is that it helps

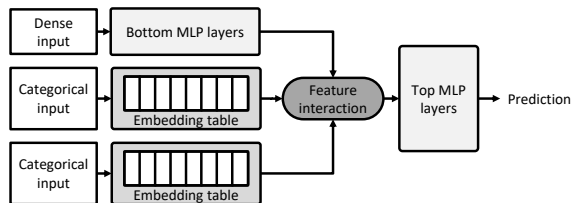


Fig. 1: A modern DNN-based RecSys model architecture.

partition a large monolithic application (in our case the model-wise replication of a RecSys inference server) into many fine-grained and loosely-coupled services. ElasticRec partitions a target RecSys model into fine-grained *model shards*, each of which is implemented as a microservice and containerized for deployment. These model shards are utilized as the unit of resource allocation which allows the container orchestration system, Kubernetes [32], to independently scale the number of shard replicas, providing high resource elasticity.

- **Utility-based resource allocation policy.** Our ElasticRec partitions the baseline monolithic RecSys model architecture into two distinct model shard types, a shard that handles dense DNN layers and sparse embedding layers. The embedding layer shard is further partitioned into hot and cold embedding shards based on the utility of embedding table entries. Such design decision opens up unique opportunities to properly align its resource allocation with its actual utility. First, ElasticRec can now selectively scale-out the number of replicas for the hot embedding shards that matches its high memory access demands. On the other hand, it also prevents ElasticRec from needlessly over-provisioning shard replicas servicing cold embeddings thereby minimizing resource waste. ElasticRec exploits these properties to design a utility-based resource allocation policy that identifies the optimal embedding table partitioning algorithm, which Kubernetes’ autoscaling policy utilizes to replicate the appropriate number of shards to fulfill a target QPS goal.

Overall, ElasticRec presents a model serving architecture for RecSys that helps customize its resource allocation best suited for its resource demand. We demonstrate that ElasticRec provides an average $3.3\times$ reduction in memory allocation size and $8.1\times$ increase in memory utility, which reduces deployment cost by an average $1.6\times$.

II. BACKGROUND

A. DNN-based Recommendation Models

Recent RecSys combines both sparse and dense features to enhance model accuracy and utilize two major components, a dense DNN layer using multi-layer perceptrons (MLP) and a sparse embedding layer (Figure 1). A sparse feature represents a categorical input (e.g., Ads a user has clicked in the past) and a dense feature represents a continuous input (e.g., user’s age). Sparse features cannot be used directly as inputs to a dense DNN layer because they represent categorical information. As such, RecSys models use *embedding tables* to translate a

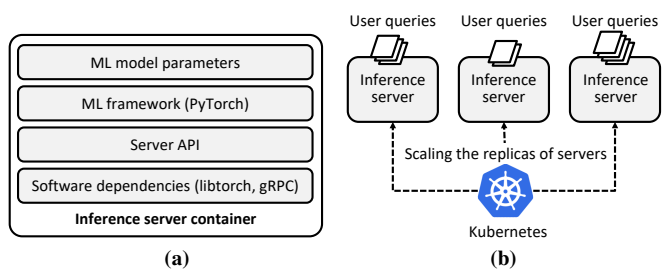


Fig. 2: (a) A containerized ML inference server using model-wise resource allocation, and (b) using Kubernetes to scale out multiple server replicas across the datacenter to meet a target QPS goal.

given sparse feature value into a dense embedding vector. An embedding table is an array of embedding vectors and a sparse feature input (which is an index ID to the embedding table) is used to read out a particular embedding vector from this table. Because the number of unique items that fall under a sparse feature category can amount to several millions to billions (e.g., number of product items sold in Amazon), an embedding table can be sized at several tens of GBs. In general, multiple embeddings are *gathered* from a given embedding table which are subsequently *pooled* into a single embedding vector using reduction operations like element-wise additions.

There are two distinguishing aspects of embedding layers vs. dense DNN layers. First, the compute intensity of embedding gather and pooling operations are extremely low, exhibiting *memory bandwidth limited* behavior, especially for embedding layers with large pooling values (number of embeddings to gather from a table). Second, because a modern RecSys model employs multiple embedding tables, deploying a RecSys model causes *high memory capacity overheads*.

B. Model Serving Architectures

ML inference server design. Current ML inference servers utilize containers [10] for their deployment because of its portability and scalability (e.g., TensorFlow Serving, Torch-Serve [48], [51]). A containerized ML inference server is packaged as a Docker image which contains all the essential ML software packages, the necessary system environment settings, and importantly the *ML model* to deploy. Because a ML model is treated as one *monolithic* application to be serviced and containers are the smallest unit of resource allocation and deployment, any given replica of the containerized inference server must contain a copy of the *entire* ML model parameters (Figure 2(a)). This paper refers to such baseline resource allocation mechanism as *model-wise* resource allocation.

Deploying inference servers at scale. The de facto standard in container orchestration is Kubernetes [32] which helps automate the deployment, scaling, and resource management of the containerized inference servers at scale (Figure 2(b)). Kubernetes cluster scheduler enables system designers to hand over the responsibility of resource management by defining deployment policies. When deploying an application, programmers can simply set the desired policy, and Kubernetes transparently manages the allocation of resources based on the specified policy. One important, automated resource man-

agement feature provided with Kubernetes is the Horizontal Pod Autoscaling (HPA) [31]. HPA automatically adjusts the number of container replicas of inference servers to satisfy a target service throughput metric (e.g., QPS) and guarantee high-quality service experience to the end users.

When a new inference server is instantiated by Kubernetes, it provisions all the resources needed for that container. As such, an initialized inference server uploads all of its ML model parameters in memory. Such model-wise allocation of resources enables each replica of the inference server to independently service user queries.

System architectures for RecSys inference server. As noted in Section II-A, the size of a single embedding table can be up to several tens of GBs. Therefore, *each inference server must be provisioned with a large enough memory to store these embedding tables*. Because high-bandwidth memory employed in GPUs are not large enough to store the entire embedding tables, modern RecSys inference servers employ CPU-only [18], [20], [21], [23], [28], [39], [49] or hybrid CPU-GPU systems [1], [7], [18], [19], [34], [35], [45], [56], [60]. Both CPU-only and CPU-GPU systems share a common property where the *memory-hungry embedding tables are stored in capacity-optimized CPU memory*.

Therefore, unlike compute-intensive DNN layers which get executed by the GPU in a CPU-GPU system (i.e., CPU-only executes DNNs using the CPU), the embedding layers are executed by the CPU in both CPU-only and CPU-GPU.

Hence, effectively utilizing CPU memory with maximum efficiency becomes vital to optimize cost. This is because the total CPU memory size determines *how many* RecSys inference servers can be deployed across the datacenter, which heavily impacts the fleet-wide QPS. In this work, we study the merits of ElasticRec’s resource allocation by using *both* CPU-only and CPU-GPU based RecSys inference servers, demonstrating its wide applicability.

C. Microservices

Microservices [44] break apart complex *monolithic* applications, whose functionality is implemented as a single service, into many *fine-grained* and *loosely-coupled* microservices. Each microservice is designed to serve a small subset of the original application’s functionality, communicating with other microservices using Remote Procedure Calls (RPC) or a RESTful API [9], [12], [26], [54]. A key advantage of microservices is its elasticity. Specifically, because the granularity in which resource allocation and scheduling are done is in individual microservices, it facilitates deploying, scaling, and updating individual microservices independently, improving the elasticity of resource allocation and its scheduling.

D. Related Work

With the growing interest in RecSys, there has been a large body of prior work exploring hardware/software optimizations for RecSys which we summarize below.

Memory bandwidth bottleneck of RecSys. As discussed in Section II-A, the embedding vector gathers and pooling

operations in RecSys incur significant memory bandwidth demands causing a bottleneck. Several prior work proposed near-/in-memory processing [4], [27], [30], [34], [35], in-storage processing [55], [57] to alleviate embedding layer’s memory bandwidth demands. Similar to our work, there are also studies that observe and utilize the skewed embedding table access pattern in RecSys for system-level optimizations. For instance, several prior studies utilize the skewed embedding access patterns to explore the efficacy of caching to reduce overall memory bandwidth demands [5], [11], [25], [27], [33], [36], [37], [41], [58], [59]. Others leverage a heterogeneous memory hierarchy [2], [3], [52], [53] to effectively lower the average latency to access slow memory. Overall, these prior work alleviates the embedding layer’s memory bandwidth requirements by exploiting the skewed access patterns. ElasticRec, on the other hand, utilizes embedding table’s unique access pattern to develop a cost-efficient, elastic resource management system.

Memory capacity bottleneck of RecSys. Kwon et al. [34], [35] proposed a disaggregated memory architecture to store large embedding tables in a remote memory node and Gouk et al. [15] explored the viability of CXL-based memory pooling for storing embedding tables. Lui et al. [39] explores the efficacy of distributed inference for RecSys where a model is partitioned and distributed across multiple machines for deployment. Such design point helps address RecSys embedding layer’s memory capacity demands by storing different embedding tables in remote CPU nodes, collecting the pooled embedding vectors using RPC calls, which is similar to ElasticRec’s microservice based design. Mudigere et al. [42] explores various model-parallel training schemes targeting embedding tables, discussing different table partitioning plans (e.g., column-wise, row-wise, table-wise partitioning) to address the memory capacity demands of RecSys training. All of these prior work strictly focus on evaluating the efficacy of their solution under a *single* inference and/or training server setting without consideration of its deployment at scale nor its resource allocation efficiencies. More importantly, the RecSys model architecture is implemented as one monolithic application, unlike ElasticRec where we focus on partitioning its implementation into fine-grained model shards using a microservice architecture to enable elastic resource scaling. DisaggRec [29] proposes a disaggregated memory system augmented with near-memory processing architectures for RecSys inference, which is designed to cost-effectively manage large embedding tables. DisaggRec addresses resource inefficiencies that arise from the varying computational and memory requirements of dense and sparse layers. Similar to [39], DisaggRec employs a distributed inference approach for RecSys and aims to tackle the resource underutilization issue by distributing the allocation of dense layers and sparse embedding layers across compute-nodes and memory-nodes, respectively, which helps improve machine utilization. Unlike ElasticRec’s dynamic, elastic resource management system, however, DisaggRec allocates a fixed amount of resources to each layer, and determining the optimal distribution of resources requires an exhaustive search. Overall, the key

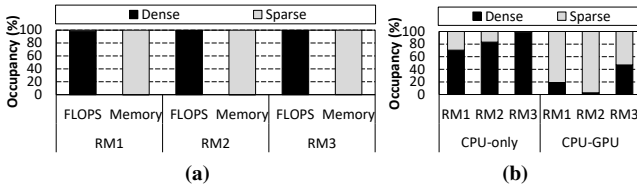


Fig. 3: The fraction of (a) FLOPs, memory consumption and (b) end-to-end inference latency (over CPU-only and CPU-GPU systems) the sparse embedding and dense DNN layers account for when evaluated over the three models studied in this paper (RM1, RM2, and RM3). FLOPs and memory consumption are architecture-independent, so its values are identical over CPU-only and CPU-GPU systems. Section V details our methodology. FLOPs percentage of sparse embedding layers in (a) are 2%, 1%, and 0.1% for RM1, RM2, and RM3, respectively. Memory consumption percentage of dense DNN layers in (a) are 0.02%, 0.02%, and 0.4% for RM1, RM2, and RM3, respectively.

contribution of ElasticRec is orthogonal to these related work.

Runtime system and scheduling for RecSys. While not necessarily employing microservices, there are several prior work suggesting RecSys optimized runtime systems or scheduling policies. Prior work [18], [20], [28] suggests multi-tenant scheduling to improve the throughput of RecSys inference servers. JiZhi [38] optimizes the serving cost of RecSys by batching the model serving pipeline. MP-Rec [22] dynamically selects the optimal hardware platform within a heterogeneous RecSys inference server containing GPUs, TPUs, and IPUs, for better performance. In general, the key contributions of ElasticRec is orthogonal to these prior work.

III. MOTIVATION

A critical limitation of model-wise allocation is that it is difficult to flexibly allocate the appropriate amount of resources to individual layers that match their utility and need, leading to resource waste. This section describes the two key factors behind baseline mechanism’s sub-optimal performance.

A. Heterogeneous Resource Demands of RecSys

The sparse embedding layer and dense DNN layer exhibit notable differences in their compute and memory characteristics, including compute intensity (FLOPs), memory footprint, and memory access pattern. Compared to large embedding tables, MLP’s model size is only in the range of several MBs, yet their compute intensity is much higher than embedding gather and pooling operations. For instance, in case of RM1 (Table II), dense DNNs account for 98% of FLOPs and 67%/19% of CPU-only/CPU-GPU’s end-to-end inference time, yet their model size only accounts for 0.02% of overall memory consumption (Figure 3). From a memory access pattern’s perspective, servicing a single query requires the entire MLP parameters to be accessed, exhibiting 100% utility of the model parameters allocated in memory. In contrast, embedding layers, due to its sparse table access patterns, exhibit extremely low memory utility as it only touches 0.001% (with a pooling factor of 100 per table) of the embedding tables per inference. This means that, on average, 99.999% of the parameters allocated in memory are of waste whenever a query is serviced.



Fig. 4: An example RecSys where the dense DNN layer exhibits half the QPS than the sparse embedding layer. (a) How the baseline model-wise resource allocation would replicate two servers to reach 100 queries/sec and (b) how our proposed ElasticRec would reach such QPS goal using fine-grained, per-layer resource allocation.

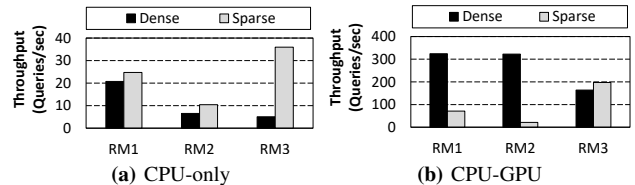


Fig. 5: Service throughput (QPS) of dense DNN and sparse embedding layers over (a) CPU-only and (b) CPU-GPU system when separately measured over the three RecSys models used in our evaluation (see Table II). As shown, due to the heterogeneous resource demands of RecSys, a significant QPS mismatch exists between sparse and dense layers, for both CPU-only and CPU-GPU system.

The mismatch in compute intensity and memory utilization, leading to significant resource waste, cannot be addressed under the baseline model-wise resource allocation. Consider the example in Figure 4 which assumes that a dense DNN and sparse embedding layer can each service 50 queries/sec and 100 queries/sec, respectively. Such mismatch in QPS is common in RecSys due to its heterogeneous model architecture (Figure 5). As the DNN layer exhibits half the QPS of the embedding layer in Figure 4, the end-to-end model-wise throughput will be bounded at 50 queries/sec. To increase the system-wide throughput to 100 queries/sec, the baseline model-wise allocation would require two replicas of the inference server to be instantiated. From a memory efficiency perspective, such model-wise replication is a significant waste as the entire embedding tables are needlessly duplicated without contributing much to improving QPS (Figure 4(a)). A more desirable solution would be to double the allocated resources *only* to the dense DNN and improve its aggregate QPS to 100 queries/sec and resolve it from being a bottleneck (Figure 4(b)). Unfortunately, fine-tuning the resource allocation separately on a per-layer basis is impossible with the baseline mechanism as each inference server is containerized as one monolithic application, forcing Kubernetes to replicate the *entire* model parameters whenever a higher system-wide QPS is desired and a new server replica is deployed.

B. Skewed Access Pattern and Locality in Embeddings

Figure 6 illustrates the access distribution of individual embedding table entries in real world RecSys datasets. As depicted, the table access pattern exhibits a power-law distribution where the majority of table accesses are covered by a very small subset of the table entries (e.g., 94% of accesses covered by only 10% of the table entries in MovieLens).

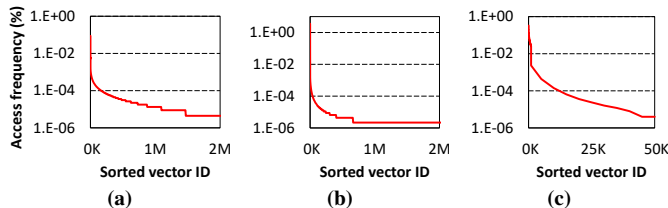


Fig. 6: Sorted access frequency of embedding vectors in real world RecSys datasets: (a) Amazon books [6], (b) Criteo [8], and (c) MovieLens [16]. The y-axis is plotted on a log-scale.

Given such property, we can infer that an embedding layer’s throughput is primarily governed by how much performance can be reaped out for embedding vector gather operations targeting those embeddings that are accessed frequently, i.e., the “hot” embeddings. To put it differently, in order to enhance the effective throughput of an embedding layer, it is more advantageous to selectively allocate more resources to embedding gathers targeting hot embeddings rather than cold embeddings. Unfortunately, as in our example in Figure 4(a), the baseline mechanism allocates resources in a coarse-grained, model-wise manner, having the entire embedding tables be replicated in memory without consideration of its actual utility.

Overall, we conclude that the baseline model-wise resource allocation does not align well with the unique properties of RecSys model serving. This misalignment leads to significant waste in memory resources, which is particularly detrimental to the memory-capacity limited embedding tables.

IV. ELASTICREC MODEL SERVING ARCHITECTURE

A. Microservice-based Inference Server Design

Server architecture overview. Figure 7 provides an overview of ElasticRec’s model serving architecture. ElasticRec employs a *microservice* programming model to break down the monolithic RecSys model serving architecture into different *model shards*, each of which is implemented as a microservice. There are two types of model shards, a dense DNN shard and a sparse embedding shard. The dense DNN shard services all the computations related to the bottom/top MLP and feature interactions (Figure 1). On the other hand, the sparse embedding shard is responsible for gathering the requested embedding vectors stored within that shard. An embedding table is partitioned into various sized embedding shards based on the hotness of embeddings. The table partitioning is done by our *dynamic programming based partitioning algorithm* (detailed in Section IV-B) which determines the optimal partitioning plan that maximizes resource efficiency.

In ElasticRec, each model shard is containerized as a Docker image. For CPU-only systems, all model shards (both dense and sparse) are CPU-centric so they are designed as containers only requiring CPU resources. As for CPU-GPU systems, the containers that service sparse embedding shards are similarly designed with only CPU resource requirements. Because of dense DNN layer’s high compute intensity and small memory footprint (Figure 3), CPU-GPU systems service dense DNN shards using a GPU-centric container utilizing both CPU/GPU

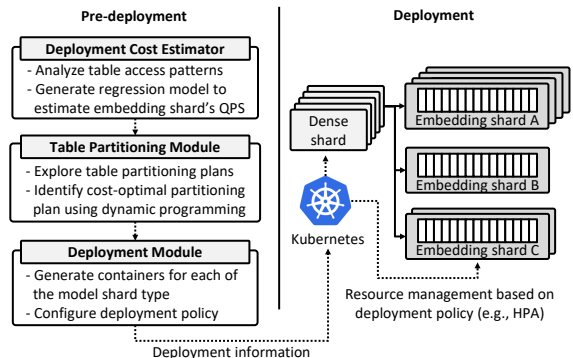


Fig. 7: High-level overview of our ElasticRec server architecture. The example assumes that ElasticRec partitions the RecSys model into one dense DNN shard and three embedding shard types, each of which is containerized for deployment. To sustain a target QPS, the example assumes that Kubernetes instantiated 5/4/1/2 replicas of the dense DNN and embedding shard A, B, and C, respectively.

resources. In our design, model shard instances communicate with each other using the gRPC protocol [17].

Life of an inference query. When a user query arrives to the inference server, the input data is routed to the dense DNN shard, which splits it into two parts: the sparse input and the dense input. The dense DNN shard then processes the bottom MLP layers using the dense input while concurrently initiating RPC calls to the sparse embedding shards to collect the required embeddings. Sending embedding gather requests across the sparse embedding shards requires a *bucketization* process that determines which among the partitioned embedding shards the input query should gather embeddings from (Section IV-C details the bucketization algorithm). The embedding shards, each storing the partitioned embedding table, gather the embeddings requested by the dense DNN shard. Once all embeddings are gathered and pooled, the sparse embedding shards send them back to the caller microservice, i.e., the dense DNN shard. Upon receiving the pooled embeddings from the sparse embedding shards, the dense shard goes through the remaining inference process including feature interaction, top MLP, and finally calculating the event probability which is returned back to the user.

Scaling out inference servers using Kubernetes. In ElasticRec, the containers that service dense and sparse model shards become the unit of resource allocation and scheduling by our container orchestration system, Kubernetes [32]. This enables ElasticRec to independently scale the number of model shard replicas to satisfy a target QPS goal, whether it be a CPU-centric shard or a GPU-centric shard, achieving high resource elasticity. Kubernetes horizontal pod autoscaling (HPA) policy defines when to scale up/down the number of shard replicas under what condition. In Section IV-D, we detail how ElasticRec utilizes such feature to adaptively adjust the shard replica numbers according to the incoming query traffic.

B. Utility-based Resource Allocation for Embeddings

The key objective of ElasticRec’s embedding table partitioning algorithm is to determine (1) the optimal number of embedding shards to partition the table and (2) how many

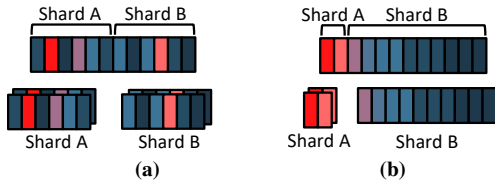


Fig. 8: Partitioning (a) an example embedding table as-is without any preprocessing, and (b) sorting the table first based on the hotness of embeddings and *then* partitioning the table into two different shards, hot (red) vs. cold (blue) embedding shards. When it comes to partitioning an embedding table, this paper always assumes that an embedding shard includes a non-overlapping set of embeddings with consecutive index IDs.

embeddings to include within each embedding shard, which minimizes its deployment cost while sustaining target QPS goals. ElasticRec proposes a *dynamic programming* (DP) based table partitioning algorithm which is based on our *profiling*-based deployment cost (i.e., memory consumption) estimation model. We discuss each of these components below.

Embedding table preprocessing. As shown in Figure 8(a), hot embeddings are randomly dispersed across the embedding table, so partitioning the table as-is into multiple shards where each shard consists of a non-overlapping set of consecutive embeddings inevitably mixes up hot and cold embeddings altogether. Such partitioning plan reduces the effectiveness of ElasticRec’s fine-grained resource allocation and scaling policy as cold embeddings will needlessly be duplicated whenever a new embedding shard is replicated.

To this end, ElasticRec first preprocesses the embedding table by sorting each embedding’s location within the table based on its access frequency. The access frequency of an embedding can be determined by keeping a history of each embedding’s access count within a given time period, one that can easily be implemented in production inference servers [37], [52]. As shown in Figure 8(b), once the table is sorted, the hottest embedding vector will be stored at the leftmost location indexed with an ID=1 and the coldest embedding located at the rightmost location indexed with ID=(number of embedding vectors in table). Using the sorted embedding table, we can now create a model shard that only includes embeddings much hotter than the other ones, which functions as a vehicle for designing our utility-based resource allocation policy, i.e., the ability to replicate a larger number of model shards *only* for the hot embeddings without duplicating cold embeddings. Note that sorting the embedding table incurs a one-time latency overhead (approximately three seconds for the largest table we evaluate) and more importantly, such preprocessing step is off the critical path of serving online inference queries.

Deployment cost estimation. Using the sorted embedding table, ElasticRec iterates through the evaluation space of various *partitioning plans* (detailed in Algorithm 2) and estimates each plan’s memory consumption to identify the optimal partitioning plan, i.e., one with the lowest memory consumption. We use Algorithm 1 to explain how ElasticRec predicts the memory consumption of a given partitioning plan, which is determined by both the size of each shard and the

Algorithm 1 Deployment Cost Estimation Algorithm

```

1: function COST(k, j)
2:   num_replicas = REPLICAS(k, j)
3:   shard_size = CAPACITY(k, j) + min_mem_alloc
4:   memory_consumption = num_replicas × shard_size
5:   return memory_consumption
6: end function

7: function REPLICAS(k, j)
8:   #  $n_t$ : average number of vectors to gather from the table
9:   #  $target\_traffic$ : predefined constant representing user_traffic
10:  #  $QPS(x)$ : Estimated QPS of a shard that gathers  $x$  embeddings,
      which is derived by our profiling-based regression model
11:  probability = CDF(j) - CDF(k)
12:   $n_s$  = probability ×  $n_t$ 
      #  $n_s$ : average number of vectors gathered from the shard
13:  estimated_QPS = QPS( $n_s$ )
14:  num_replicas = target_traffic/estimated_QPS
15:  return num_replicas
16: end function

17: function CAPACITY(k, j)
18:   return  $(j - k + 1) × (size\_of\_a\_single\_embedding\_vector)$ 
19: end function

```

number of replicas to instantiate for each shard (line 4).

The number of shard replicas to instantiate can be estimated by dividing up the target QPS with the number of queries a specific shard is able to process per second (line 14). We observe that the QPS an embedding shard can sustain is primarily determined by two key parameters: (1) the number of embeddings to gather from that shard and (2) the size of each embedding vector which determines the overall volume of data to fetch from memory. We employ a *profiling-based* approach to estimate these parameters as explained below. Suppose the number of vectors to gather from the original, non-partitioned embedding table is defined as n_t (line 8). We first need to predict how many embeddings will be gathered from the partitioned embedding shard (n_s) out of the overall n_t . The value of n_s can be estimated by predicting what fraction of the overall table accesses (n_t) is likely to fall under the given embedding shard. Since the embedding vector’s access frequency (one which we already used to sort and preprocess the table) is a direct indicator of which embeddings are most likely to be accessed to service a query, we construct a CDF (cumulative distribution function) using the “sorted” embedding table’s access frequency information. Because ElasticRec constructs embedding shards over non-overlapping set of embedding vectors with consecutive index IDs (Figure 8(b)), an embedding shard starting from index ID k to j ($k < j$) is likely to account for $(CDF(j) - CDF(k))$ percentage of n_t gathers (line 11). By multiplying this probability with n_t , we get a reliable estimation of the value of n_s (line 12).

Now that we have determined the number of embeddings to gather from a shard (n_s), we discuss how to predict the estimated QPS for that shard. The QPS of an embedding gather operation is determined not only by the number of embeddings to gather from that shard but also the underlying hardware architecture the gather operation is initiated. Given such, ElasticRec conducts a one-time profiling of embedding

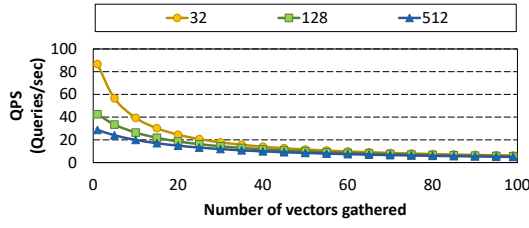


Fig. 9: The changes in QPS (y-axis) as a function of the number of embedding gathers (x-axis) conducted over a 20M entry embedding table. We change the size of the embedding vector dimension (from 32 to 512 element vector) to illustrate how different data volume sizes that are fetched from memory impact the QPS, i.e., the larger the dimension size, the smaller its QPS due to higher read traffic.

vector gather operations, swept over various number of vector gathers, and measures its QPS to construct a lookup table indexed by the number of gathers (Figure 9). We utilize this profiled lookup table to generate a regression model ($QPS(x)$ in line 10, 13) that estimates the QPS of an embedding gather operator as a function of n_s . The estimated QPS of a shard is utilized to determine the number of replicas required to meet a target QPS goal (line 14). As for the target QPS goal in line 14, it serves as a constant value for the dynamic programming algorithm as all the partitioning plans share the same QPS values. Any QPS values that make the number of replicas larger than 1 can be utilized for the target QPS. Here, we utilized 1000 for the QPS goal. Since each shard’s memory consumption (line 3) is determined by the embedding shard size (line 18) and other minimally required memory allocations for each container (e.g., code, input buffers, `min_mem_alloc` in line 3), we multiply the number of replicas (line 2) with per-shard memory consumption (line 3) to get an estimated memory consumption for deploying that shard (line 4).

DP-based table partitioning algorithm. DP is a problem-solving technique that breaks up a complex problem into a set of sub-problems. DP expresses the solution to the complex problem *recursively* in terms of the sub-problems and solving the recursive relation without repeatedly solving the same sub-problem twice by *memoizing* previously solved sub-problems. We use Figure 10 to explain how DP sub-problems are defined and solved for embedding table partitioning.

Consider an embedding table E having N_{max} embedding vectors already sorted based on their hotness as discussed in Figure 8(b). We define $Mem[num_shards][x]$ as the lowest memory cost incurred when a table E' containing only the x most hot embeddings of table E (i.e., $x \leq N_{max}$, so when x equals N_{max} , E' is equivalent to E) is partitioned into num_shards shards. In Figure 10, for instance, E is a table with a total of $N_{max}=5$ embeddings. Also, $Mem[2][3]$ stores the smallest memory cost of partitioning the table E' sized with 3 most hot embeddings of E (i.e., $E[1,2,3]$) into $num_shards=2$ shards. The key objective of ElasticRec’s DP algorithm is to iterate through the problem space of $Mem[num_shards][x]$ and identify the value of num_shards and its partitioning plan that results in the least memory consumption.

In Figure 10, we illustrate the process of deriving $Mem[3][5]$, which represents the minimum memory cost when

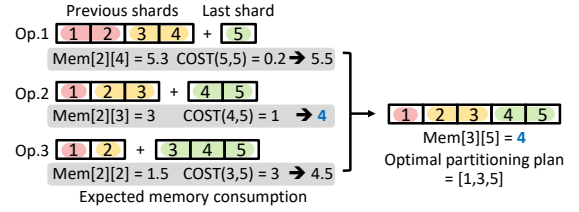


Fig. 10: Example of how our DP algorithm evaluates $Mem[3][5]$ and its optimal partitioning plan. Different shards are colored differently (red/yellow/green). For clarity of explanation, this example assumes that $COST(k,j)$ is defined as a simple function (unlike Algorithm 1) that returns a value equal to $(j - i + 1)^2/i$. For instance, $COST(4,5) = (5 - 4 + 1)^2/4 = 1$.

Algorithm 2 Embedding Table Partitioning Algorithm

```

1: function FIND_OPTIMAL_PARTITIONING_PLAN
  #  $Mem[num\_shards][x]$ : The smallest memory cost when partitioning
  # the table  $E'$  including  $x$  most hot embeddings to  $num\_shards$  shards
  #  $COST(start\_ID, end\_ID)$ : Expected memory consumption of a
  # shard that contains embeddings with ID from  $start\_ID$  to  $end\_ID$ 
2: for  $end\_ID = 1$  to  $N_{max}$  do
3:    $Mem[1][end\_ID] = COST(1, end\_ID)$ 
4: end for
5: for  $num\_shards = 2$  to  $S_{max}$  do
6:   for  $end\_ID = num\_shards$  to  $N_{max}$  do
7:      $min\_estimation = float(inf)$ 
8:     for  $start\_ID = num\_shards$  to  $end\_ID$  do
9:        $prev\_shards\_mem = Mem[num\_shards-1][start\_ID - 1]$ 
10:       $last\_shard\_mem = COST(start\_ID, end\_ID)$ 
11:       $cur\_estimation = prev\_shards\_mem + last\_shard\_mem$ 
12:      if  $cur\_estimation < min\_estimation$  then
13:         $min\_estimation = cur\_estimation$ 
14:        Memoize current partitioning points
15:      end if
16:    end for
17:     $Mem[num\_shards][end\_ID] = min\_estimation$ 
18:  end for
19: end for
20: return partitioning points corresponding to smallest Mem value
21: end function

```

the table E is partitioned into three shards. Each partitioning plan’s memory consumption is the summation of two values: (1) the estimated memory consumption of the first two shards (red/yellow) and (2) the third (green) shard’s memory consumption. Because of the recursive relationship in DP, the optimal memory consumption for the first two shards can be determined by referencing the memoized value of $Mem[2][x]$ ($x=4/3/2$), which represents the least memory consumed when E' is partitioned into two shards. Since the memory consumption of the third (green) shard can be evaluated using the $COST$ function (Algorithm 1), we arrive at the estimated memory consumption of option 1/2/3 as shown in Figure 10. By comparing the estimated memory consumption for each partitioning option, we can identify the optimal solution to this problem (option 2) that incurs the lowest memory cost. In the given example, the first two (red/yellow) shards partitioned with $Mem[2][3]$ (i.e., red and yellow shards containing $E[1]$ and $E[2,3]$ embeddings respectively) and having the third (green) shard include the remaining two embeddings ($E[4,5]$) yields the least memory consumption. Thus, $Mem[3][5]$ is updated with a memory cost

of 4 and the *partitioning points* of [1, 3, 5] (which stores the last index ID of each shard) is separately stored as the corresponding, optimal partitioning plan for this example.

In Algorithm 2, we detail ElasticRec’s table partitioning algorithm, which is a generalization of the aforementioned example. The initialization step of our DP algorithm partitions the table into a single shard. Here the values of $\text{Mem}[1][\text{end}_{ID}]$ represent the optimal memory consumption when a single shard contains the end_{ID} most hot embeddings (line 2-4), one which is derived using our COST function (Algorithm 1). The remaining $\text{Mem}[\text{num}_{shards}][\text{end}_{ID}]$ values are derived by exploiting the recursive relation between the table partitioned with $(i - 1)$ shards and the table partitioned with i shards where the optimal Mem value for the $(i - 1)$ shards can always be retrieved through the memoized solution, without re-computation (line 9). Similar to the example in Figure 10, we iterate through all possible shard sizes for the last shard by changing start_{ID} , from num_{shards} to end_{ID} (line 8), and evaluate its COST function (line 10) in order to determine the overall minimum memory consumption under that partitioning plan (line 17). After the entire design space of $\text{Mem}[-][\text{end}_{ID}]$ is evaluated up to maximum possible number of shards (S_{max}), the one with the minimum memory cost is chosen as the final partitioning plan (i.e., the number of shards to partition the original table and its partitioning points).

The cost of our DP algorithm is $O(S_{max} \times N_{max})$ which can be calculated within 18 seconds for an embedding table with 20M entries. Importantly, executing the DP algorithm is off the critical path of serving online inference queries.

C. Bucketization

Since ElasticRec partitions an embedding table into multiple embedding shards, the index IDs used to lookup the original embedding table should be remapped appropriately, in accordance to the partitioned embedding shards. We refer to such process as *bucketization* which we explain below.

Consider the example in Figure 11 which assumes that a table with 10 embeddings are partitioned into two shards. To improve throughput, a single query contains multiple inputs that are batched together for concurrent processing. As such, when accessing an embedding table, two arrays are utilized, the index array and the offset array. The index array stores the list of IDs to lookup from the table, whereas the offset array is used to separate out which elements within the index array should different inputs within the query utilize. In Figure 11(a), for instance, the first element in the offset array (value 0, red) indicates that input 0 requires index IDs starting from offset 0 of the index array, whereas input 1 should utilize IDs starting from offset 2 (gray) of the index array. Since these two arrays can no longer be used as-is to access the partitioned embedding shards, our proposed algorithm bucketizes the original input into two partitions as follows. First, it iterates through the original index array (and offset array) and determines which embedding shard each embedding should be gathered from, generating the intermediate index and offset arrays as shown in Figure 11(b). The values stored in

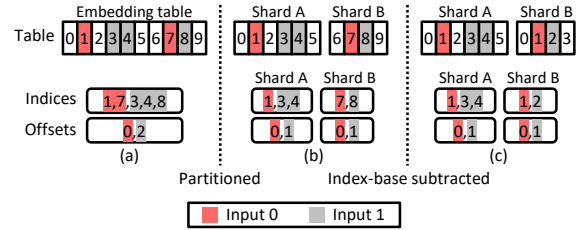


Fig. 11: An example bucketization process that partitions a 10 element table into two shards. Indices and offsets used for input 0 and 1 are highlighted in red and gray, respectively.

shard B’s index array is then subtracted by 6 (i.e., the size of the first shard A) so that the index IDs used to lookup the sharded table can start from a base value of 0. The bucketization algorithm is simple to implement and highly parallelizable. We omit the pseudo-code that summarizes its implementation for brevity.

D. Deploying ElasticRec at Scale using Kubernetes

Since each model shard is encapsulated as a container, Kubernetes can independently scale each shard replicas as dictated by the HPA policy. We employ a throughput-centric metric as the HPA target for sparse shards while a latency-centric metric is used for dense shards’ HPA target.

For sparse shards, we utilize shard’s maximum QPS as the autoscaling target. Specifically, ElasticRec measures the maximum QPS each sparse shard can sustain (QPS_{max}), stress-testing each one of them by gradually increasing input query traffic intensity and monitoring at which point the tail latency increases rapidly. ElasticRec then configures the HPA policy to have each sparse shard’s respective QPS_{max} value be set as the threshold to trigger each sparse microservice to replicate an additional shard instance. For dense shards, we define a latency threshold where the auto-scaling HPA target is set to 65% of the SLA, ensuring that service latency remains within acceptable bounds and does not lead to SLA violations. Overall, ElasticRec can adaptively adjust the replicas of each shard type that satisfies the demands of incoming query traffic while also achieving high memory efficiency.

V. EVALUATION METHODOLOGY

A. Hardware Architecture

CPU-only inference server. In Section VI, we first evaluate ElasticRec over CPU-only systems using a multi-node CPU cluster consisting of one master node and eleven compute nodes. Each compute node’s configuration is in line with those employed in production CPU-only RecSys inference servers [20]. Specifically, each CPU node is equipped with a dual-socket Intel Xeon Gold 6242 Skylake CPU containing 32 logical cores and 192 GB of DRAM per socket, each socket providing 128 GB/sec of memory bandwidth. The compute nodes communicate over a 10 Gbps network.

CPU-GPU inference server. We also evaluate ElasticRec’s applicability over CPU-GPU systems using Google Kubernetes Engine (GKE) in Google Cloud [14]. In this setup, we utilize a GKE cluster that contains twenty hybrid CPU-GPU

TABLE I: The key parameters changed in our microbenchmark based evaluations in Section VI-A. The default RecSys model configuration for our microbenchmark is based on DLRM RM1 (Table II).

Configurations			
MLP layer size	Light	Medium	Heavy
	Bottom: 64-32-32 Top: 64-32-1	Bottom: 256-128-32 Top: 256-64-1	Bottom: 512-256-32 Top: 512-64-1
Locality	Low	Medium	High
	P: 10%	P: 50%	P: 90%
Table (N)	Total number of embedding tables: 1, 4, 10, 16		
Shard	Number of shards to partition the table: 1, 2, 4, 8, and 16		

compute nodes (n1-standard-32 node [13] containing 32 CPU logical cores and 120 GB of DRAM, and connected to an NVIDIA Tesla T4 GPU [47] over PCIe). The compute nodes communicate over a 32 Gbps network.

B. Software Architecture

Each model shard communicates with one another using C++ gRPC protocol. RecSys models are designed using PyTorch’s libtorch (v1.12) and the DLRM GitHub repository [40]. Resource management is handled by Kubernetes (v1.26), which is responsible for scaling in/out each model shard replicas according to input query traffic. Load balancing is managed using Linkerd (v2.12), routing the input queries to the shard replicas as appropriate. We also use a Prometheus metrics server [50] to collect various custom statistics, e.g., CPU usage, memory consumption, tail latency, and QPS.

C. Workloads

To better illustrate ElasticRec’s effectiveness on model serving, we use both microbenchmarks (Table I) and state-of-the-art RecSys model configurations (Table II) used in prior work.

Microbenchmarks. We construct several microbenchmarks using DLRM’s RM1 (Table II) as our default model configuration. The microbenchmarks are designed to better cover the large evaluation space by changing some of its key model parameters in terms of (1) the dense MLP layer size, (2) embedding table’s locality, (3) number of tables, and (4) the number of shards to partition a table (Table I). We use these microbenchmarks to evaluate the sensitivity of ElasticRec across a wide range of DLRM configurations, focusing on ElasticRec’s effectiveness in reducing memory allocation size.

State-of-the-art RecSys workloads. We also evaluate ElasticRec across multiple dimensions in detail using three representative DLRM configurations (Table II) used in prior work [18], [20], [28], [39], [42], [43]. The SLA target is set to 400ms to be consistent with industry recommendations on SLA for RecSys, which is several hundreds of milliseconds [18]. All experiments are collected while ensuring that the 95 percentile tail latency does not violate SLA.

Query modeling. A query consists of multiple items to be ranked for a given user, thus the size of a query determines the input batch size. We follow the methodology from prior work [18] to model the query distribution by setting the batch size as 32. To model the effect of locality on embedding table accesses, we introduce a locality metric P , which indicates the

TABLE II: State-of-the-art RecSys workload configurations.

	RM1	RM2	RM3
Bottom MLP	256-128-32	256-128-32	2560-512-32
Top MLP	256-64-1	512-128-1	512-128-1
Number of embeddings	20M	20M	20M
Number of tables	10	32	10
Embedding dimension	32	32	32
Number of embedding gatherers	128	128	32
Locality (P)	90%	90%	90%

percentage of total accesses that are captured by the top 10% most frequently accessed vectors (e.g., $P=94\%$ for MoveLens dataset, indicating that 94% of embedding table lookups are covered by the top 10% hottest embeddings). Table I and Table II shows the P values in our evaluated microbenchmarks and state-of-the-art RecSys workloads.

VI. EVALUATION

This section evaluates ElasticRec over both CPU-only and CPU-GPU systems. For brevity and clarity of explanation, we focus our evaluation over CPU-only systems when studying our microbenchmarks in Section VI-A. We then evaluate state-of-the-art RecSys workloads over CPU-only and CPU-GPU systems in Section VI-B and Section VI-C, respectively.

A. Microbenchmarks

MLP layer size. When the number of parameters in MLP layers is increased (from “Light” to “Heavy” in Figure 12(a)), the MLP layers become more compute-intensive and experiences lower QPS. To meet the target system-wide QPS goal, model-wise allocation must instantiate additional server replicas which in turn ends up duplicating the entire embedding tables. Consequently, as the MLP layer’s compute requirement increases, the overall memory consumption under model-wise allocation also increases rapidly. In contrast, when the MLP size is increased to “Heavy”, ElasticRec is able to provision additional resources only to the bottlenecked MLP layers, allowing only a modest increase in memory consumption.

Locality in embedding tables. We discussed in Section IV that ElasticRec can allocate more resources only to those embedding shards that are accessed more frequently. As shown in Figure 12(b), when the locality in table accesses is “High”, ElasticRec instantiates a larger number of replicas for the hot embedding shards while spawning a relatively smaller number of cold embedding shards. Such feature helps ElasticRec minimize wasted memory resources allocated for servicing embedding that are not accessed frequently, achieving $2.2\times$ memory consumption savings when locality is “High”. The baseline model-wise allocation, on the other hand, is not able to save memory allocations at all by exploiting the table’s locality, experiencing almost a constant memory consumption regardless of the level of locality.

Total number of tables. Recent large-scale RecSys model architectures contain a large number of sparse features, which translates into a large number of embedding tables. The microbenchmarks in Figure 12(c) is designed to demonstrate the scalability of ElasticRec’s table partitioning algorithm when the number of tables is increased (the experiment assumes that

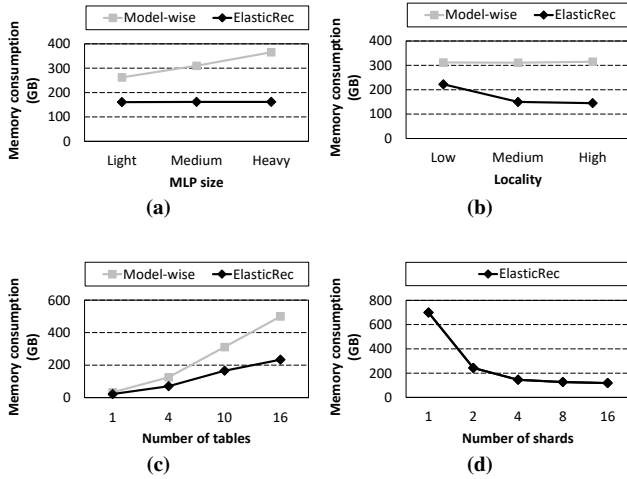


Fig. 12: Memory consumption in our microbenchmarks, exploring the impact of (a) MLP size, (b) embedding table locality, (c) number of tables, and (d) the number of shards to partition a table.

all tables are sized identically, i.e., the larger the number of tables, the larger its aggregate memory consumption). When a model contains multiple tables, ElasticRec applies its table partitioning algorithm separately for each individual table. For instance, if ElasticRec’s partitioning algorithm decides that an embedding table should be partitioned into 4 shards and there exists 10 tables, a total of 40 shards (4 shards \times 10 tables) will be generated, each of which will be subject for resource allocation independently by Kubernetes. Such fine-grained resource management provides ElasticRec with high scalability to multiple tables, showing a large performance gap against baseline model-wise allocation.

Number of shards to partition a table. In Section IV-B, we discussed how our table partitioning algorithm identifies the optimal number of shards to partition a table. To demonstrate the effectiveness of ElasticRec’s table partitioning, Figure 12(d) shows the overall memory consumption when we manually change the number of partitioned shards. As depicted, as the number of shards increases, the memory consumption generally decreases. Note that the memory consumption plateaus at 4 shards, a point which ElasticRec’s table partitioning algorithm also determines as the optimal partitioning plan to minimize memory consumption. As discussed in Section IV-B, every container replica incurs a minimally required memory consumption (e.g., code, input buffers) to prevent containers from an out-of-memory error. As such, having an excessively large number of container replicas adds high memory overheads, leading to diminishing returns.

B. State-of-the-art RecSys Workloads (CPU-only)

Memory consumption. Figure 13 shows the overall memory consumption when both model-wise allocation (denoted “MW”) and ElasticRec allocate server resources to meet the same target QPS goal. For each of RM1, RM2, and RM3, ElasticRec’s partitioning algorithm decides to partition the embedding tables into 4, 3, and 3 shards, respectively. As such,

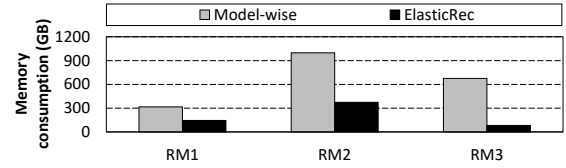


Fig. 13: CPU-only system’s memory consumption over three state-of-the-art RecSys models (100 queries/sec).

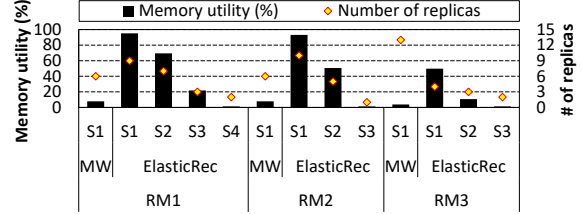


Fig. 14: CPU memory utility (left axis) and number of shard replicas instantiated to meet target QPS (right axis) in CPU-only system.

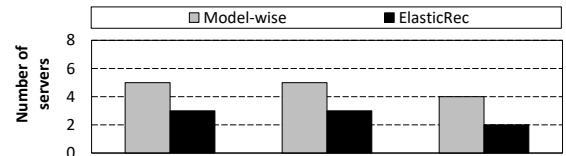


Fig. 15: The number of CPU server nodes required to meet the same QPS target (100 queries/sec) in CPU-only system.

a total of 40 shards (4 shards \times 10 tables), 96 shards (3 shards \times 32 tables), and 30 shards (3 shards \times 10 tables) for RM1, RM2, and RM3 (see Table II) are generated for each model’s deployment, allowing Kubernetes to flexibly tune the number of shard replicas in a fine-grained manner. Overall, ElasticRec shows substantial reduction in memory usage, achieving 2.2 \times , 2.6 \times , 8.1 \times reduction in memory consumption. Note that ElasticRec’s memory saving is particularly significant for RM3. This is because the MLP layers in RM3 are much more compute-intensive than the other two models, causing the model-wise allocation to replicate a larger number of inference servers as a whole (detailed later in Figure 14) and suffer more from needless duplication of cold embedding vectors.

Memory utility. ElasticRec’s significant memory reduction can be attributed to intelligently allocating memory resources based on its actual utility. We demonstrate how well memory is utilized by measuring the percentage of embeddings that are actually accessed within a shard while servicing the first 1,000 queries. Figure 14 illustrates the memory utility of each embedding shard. For brevity, we only show the utility of the first embedding table from each workload. Each embedding shard is denoted as $S(N)$, where N represents the shard ID. For ElasticRec, embedding shards with a smaller ID contains hotter embeddings (e.g., embeddings in $S1$ are hotter than those in $S2$). Because model-wise allocation does not partition the embedding tables, a single embedding shard exists that includes the entire embeddings (denoted $S1$ under “MW”). On average, model-wise allocation achieves only 6% of memory utility. Despite such low memory utility, model-wise allocation must replicate the entire inference server to meet target QPS,

substantially wasting memory. Such problem becomes especially more pronounced for the compute-intensive RM3, leading to a large number of replicated servers and high memory consumption (as discussed in Figure 13). With our ElasticRec, hotter shards consistently exhibit higher memory utility. More importantly, the number of shard replicas is proportional to the hotness of each individual shard, allowing *memory resources to be preferentially allocated to those shards that will actually utilize it efficiently*. Overall, ElasticRec achieves an average $8.1\times$ higher memory utility.

Cost. We quantify ElasticRec’s cost savings by measuring the total number of CPU servers required to satisfy the same target throughput of 100 QPS (Figure 15). While the additional communication overheads of ElasticRec adds 31 ms of average latency (8% of SLA), our proposal demonstrates its efficiency by cutting down the number of deployed servers ($1.67\times$, $1.67\times$, $2.0\times$ reduction vs. model-wise allocation for RM1/2/3, respectively) and substantially reducing cost by an average $1.7\times$ vs. model-wise allocation. These results highlight the practical benefits and cost-efficiency of ElasticRec’s utility-based resource allocation.

C. State-of-the-art RecSys Workloads (CPU-GPU)

We now demonstrate ElasticRec’s effectiveness over CPU-GPU systems. In ElasticRec, containers that service sparse embedding shards are designed with only CPU resource requirements while compute-intensive dense DNN shards are designed as GPU-centric containers utilizing *both* GPU and CPU resources. The baseline model-wise allocation, on the other hand, encapsulates all CPU (sparse embedding layers) and GPU (dense DNN layers) resources in a single container, having coarse-grained resource allocation. Below we evaluate ElasticRec’s effect on memory consumption/utility and cost.

Memory consumption. In our CPU-GPU server, the CPU architecture specification is different vs. our CPU-only setting (Section V-A). As such, ElasticRec’s partitioning algorithm decides to partition all the embedding tables into 3 shards per table for all three models, amounting to a total of 30 shards, 96 shards, and 30 shards for RM1, RM2, and RM3, respectively. Figure 16 summarizes ElasticRec’s effect on memory consumption. It is worth pointing out that the benefit of ElasticRec’s memory consumption saving for RM3 ($2.6\times$ reduction) is less pronounced compared to CPU-only systems ($8.1\times$ reduction). RM3 has relatively larger MLP layers than RM1/2 so it leads to lower QPS in a CPU-only system, necessitating a larger number of replicas to fulfill its compute/memory demands. With CPU-GPU systems, these compute-intensive dense DNNs are offloaded to the GPU and are executed more efficiently, requiring less replicas. As such, the inefficiency of duplicated resource allocation is alleviated under CPU-GPU systems which leads to a smaller gap in memory consumption between baseline and ElasticRec. Nonetheless, ElasticRec still shows significant reduction in memory usage, achieving $2.7\times$, $3.6\times$, $2.6\times$ smaller memory allocation size.

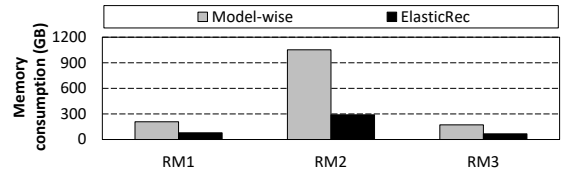


Fig. 16: CPU-GPU system’s memory consumption over three state-of-the-art RecSys models (200 queries/sec).

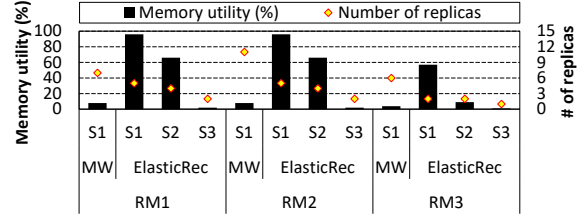


Fig. 17: CPU memory utility (left axis) and number of shard replicas instantiated to meet target QPS (right axis) in CPU-GPU system.

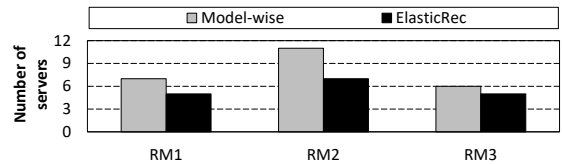


Fig. 18: The number of CPU-GPU server nodes required to meet the same QPS target (200 queries/sec) in CPU-GPU system.

Memory utility. Similar to CPU-only systems, baseline model-wise allocation still suffers from significant memory underutilization averaging 6% memory utility (Figure 17). ElasticRec again demonstrates its effectiveness in improving memory utility where hotter shards consistently exhibit higher memory utility. Furthermore, the number of shards replicated is proportional to the hotness of each individual shard, making sure that memory resources are allocated to those shards that actually utilize it efficiently. On average, ElasticRec achieves an average $8\times$ higher memory utilization.

Cost. Figure 18 shows the number of CPU-GPU server nodes needed to reach a target throughput of 200 QPS. While the additional communication overheads of ElasticRec adds 60 ms of average latency (15% of SLA), ElasticRec requires $1.4\times$, $1.6\times$, $1.2\times$ fewer servers for RM1, RM2, and RM3, respectively, than baseline model-wise allocation. Overall, these results highlight the wide applicability of ElasticRec across different hardware platforms.

D. Effectiveness to dynamic input query traffic

At-scale datacenters have a constantly changing input query traffic, necessitating Kubernetes to adaptively adjust the number of inference server replicas to deploy. In Figure 19, we demonstrate the robustness of ElasticRec to dynamically changing target QPS goals when executing RM1. We collect the resulting QPS achieved with baseline and ElasticRec, its memory consumption, and tail latency. The input query traffic is changed in a total of 5 increments, from Time=5 until Time=20, and then decreased at Time=24. As the input traffic changes, Kubernetes scales in/out the number of replicas based

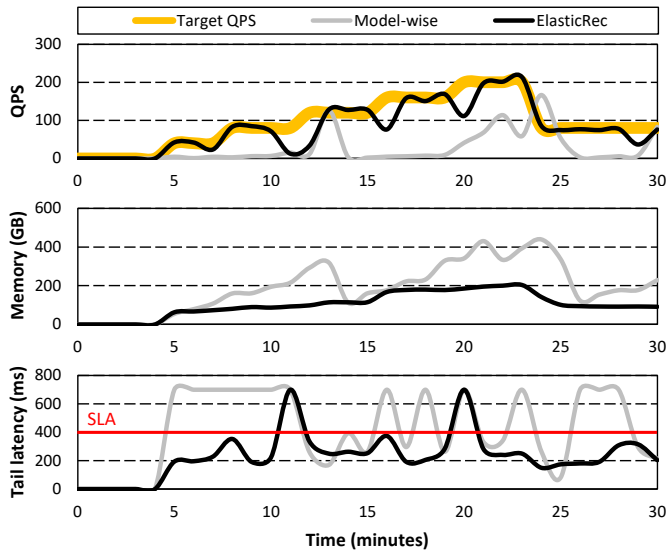


Fig. 19: Changes in QPS, memory consumption, and tail latency in response to the fluctuation in input traffic. The yellow line represents the target QPS in response to the input traffic. As discussed in Section V, the SLA target is set to 400ms. For brevity, we only show the results over a CPU-only system.

on the underlying HPA policy. For every change in target QPS, ElasticRec’s achieved QPS slightly drops in response to the traffic change and the accompanied change in the deployed shard replicas. However, after the shard replicas are appropriately provisioned, ElasticRec is able to quickly reach the target QPS goal while also meeting the tail latency in a stable manner. The baseline model-wise allocation, on the other hand, exhibits several shortcomings as follows. First, the amount of memory allocated is significantly higher with baseline, reaching $3.1\times$ higher memory consumption than ElasticRec at its peak usage. Second, model-wise allocation responds much more slowly than ElasticRec to reach the target QPS (e.g., the QPS of model-wise starts to increase at around Time=20), exhibiting much more frequent spikes in tail latency that violates SLA (400ms). These drawbacks arise because the granularity of resource allocation is much more coarse-grained under model-wise allocation, taking more time to initialize an inference server, load the model parameters into memory, and get ready to service queries. Overall, these experiments illustrate the ElasticRec’s ability to effectively adjust its resource allocation to the dynamically fluctuating input query traffic.

E. ElasticRec vs. GPU Embedding Caches

As mentioned in Section II-D, there exists prior work that utilizes the skewed embedding table access patterns to cache hot embedding vectors inside a GPU-side embedding cache, which helps alleviate the CPU memory bandwidth pressure of embedding table lookups and increase embedding layer’s throughput. In this section, we compare ElasticRec’s fine-grained resource management vs. baseline monolithic model-wise resource management augmented with a GPU-side embedding cache. In Figure 20, the baseline model-wise allocation

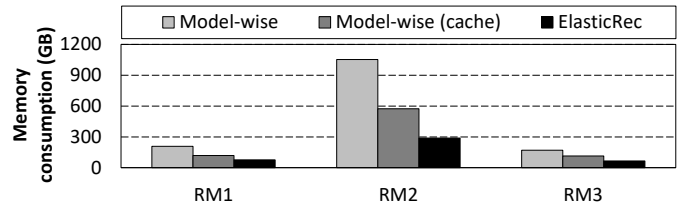


Fig. 20: CPU-GPU system’s memory consumption (200 queries/sec).

augmented with a GPU embedding cache is denoted as “model-wise (cache)”. Depending on the size of the GPU-side embedding cache (which must be implemented inside GPU’s capacity-constrained HBM), the amount of embedding table lookup operations captured within the GPU’s embedding cache (HBM) can vary significantly (e.g., [36] reports that a GPU-side embedding cache that uses up to 20% of GPU’s 32 GB HBM can capture 40% to 90% of embedding table accesses in GPU memory). The purpose of this study is to evaluate the implication of GPU-side embedding cache on memory consumption savings and its overall competitiveness vs. ElasticRec, so we conservatively model the baseline “model-wise (cache)” as follows. Following the methodology by Kwon et al. [36] we assume that model-wise (cache) contains a large enough cache to always capture 90% of its embedding gather operations within GPU’s local memory while the remaining 10% of embedding gathers are serviced from the CPU. Compared to baseline model-wise, model-wise (cache) is able to reduce the average latency for embedding layer’s execution by 47%, leading to an increase in each shard instance’s throughput and thereby reducing the total system-wide memory consumption by 41%. However, the challenges of the coarse-grained model-wise resource allocation still remains with model-wise (cache), allowing ElasticRec to reduce overall memory consumption by $1.7\times$ vs. model-wise (cache).

VII. CONCLUSION

We present ElasticRec, a RecSys model serving architecture providing resource elasticity and high memory efficiency. ElasticRec overcomes the limitations of conventional model-wise resource allocation by employing a microservice software architecture to partition a RecSys model into fine-grained model shards, which act as the unit of resource allocation. By independently scaling the number of shard replicas, we demonstrated how ElasticRec effectively addresses the heterogeneous resource demands of sparse and dense layers in RecSys.

ACKNOWLEDGEMENTS

This work was supported by the National Research Foundation of Korea (NRF) grant funded by the Korea government (MSIT) (NRF-2021R1A2C2091753). Minsoo Rhu is the corresponding author.

REFERENCES

- [1] B. Acun, M. Murphy, X. Wang, J. Nie, C.-J. Wu, and K. Hazelwood, “Understanding training efficiency of deep learning recommendation models at scale,” in *Proceedings of the International Symposium on High-Performance Computer Architecture (HPCA)*, 2021.

- [2] M. Adnan, Y. E. Maboud, D. Mahajan, and P. J. Nair, "Accelerating Recommendation System Training by Leveraging Popular Choices," in *Proceedings of the VLDB Endowment*, 2021.
- [3] E. K. Ardestani, C. Kim, S. J. Lee, L. Pan, J. Axboe, V. Rampersad, B. Agrawal, F. Yu, A. Yu, T. Le et al., "Supporting Massive DLRM Inference Through Software Defined Memory," in *Proceedings of the IEEE International Conference on Distributed Computing Systems (ICDCS)*, 2022.
- [4] B. Asgari, R. Hadidi, J. Cao, S.-K. Lim, H. Kim et al., "FAFNIR: Accelerating Sparse Gathering by Using Efficient Near-Memory Intelligent Reduction," in *Proceedings of the International Symposium on High-Performance Computer Architecture (HPCA)*, 2021.
- [5] K. Balasubramanian, A. Alshabanah, J. D. Choe, and M. Annavaram, "cDLRM: Look Ahead Caching for Scalable Training of Recommendation Models," in *Proceedings of the ACM Conference on Recommender Systems (RecSys)*, 2021.
- [6] Bekheet, Mohamed, "Amazon Books Reviews Dataset," <https://www.kaggle.com/datasets/mohamedbakhet/amazon-books-reviews>, 2022.
- [7] H.-T. Cheng, L. Koc, J. Harmsen, T. Shaked, T. Chandra, H. Aradhye, G. Anderson, G. Corrado, W. Chai, M. Ispir, R. Anil, Z. Haque, L. Hong, V. Jain, X. Liu, and H. Shah, "Wide & Deep Learning for Recommender Systems," in *Proceedings of the 1st workshop on deep learning for recommender systems*, 2016.
- [8] Criteo, "Display Advertising Challenge," <https://www.kaggle.com/c/criteo-display-ad-challenge>, 2014.
- [9] N. Dmitry and S.-S. Manfred, "On Micro-Services Architecture," *International Journal of Open Information Technologies*, 2014.
- [10] Docker, "What is a Container?" <https://www.docker.com/resources/what-container/>, 2023.
- [11] A. Eisenman, M. Naumov, D. Gardner, M. Smelyanskiy, S. Pupyrev, K. Hazelwood, A. Cidon, and S. Katti, "Bandana: Using Non-Volatile Memory for Storing Deep Learning Models," *Proceedings of Machine Learning and Systems (MLSys)*, 2019.
- [12] X. Feng, J. Shen, and Y. Fan, "REST: An Alternative to RPC for Web Services Architecture," in *International Conference on Future Information Networks*, 2009.
- [13] Google Cloud, "General-purpose Machine Family for Compute Engine," <https://cloud.google.com/compute/docs/general-purpose-machines>, 2023.
- [14] Google Cloud, "Google Kubernetes Engine (GKE)," <https://cloud.google.com/kubernetes-engine>, 2023.
- [15] D. Gouk, S. Lee, M. Kwon, and M. Jung, "Direct Access, {High-Performance} Memory Disaggregation with {DirectCXL}," in *Proceedings of USENIX Annual Technical Conference*, 2022.
- [16] GroupLens, "MovieLens Dataset," <https://grouplens.org/datasets/movie-lens/>, 2019.
- [17] gRPC, "gRPC: A High Performance, Open Source Universal RPC Framework," <https://grpc.io/>, 2023.
- [18] U. Gupta, S. Hsia, V. Saraph, X. Wang, B. Reagen, G.-Y. Wei, H.-H. S. Lee, D. Brooks, and C.-J. Wu, "DeepRecSys: A System for Optimizing End-to-end At-scale Neural Recommendation Inference," in *Proceedings of the International Symposium on Computer Architecture (ISCA)*, 2020.
- [19] U. Gupta, S. Hsia, J. Zhang, M. Wilkening, J. Pombra, H.-H. S. Lee, G.-Y. Wei, C.-J. Wu, and D. Brooks, "RecPipe: Co-Designing Models and Hardware to Jointly Optimize Recommendation Quality and Performance," in *Proceedings of the International Symposium on Microarchitecture (MICRO)*, 2021.
- [20] U. Gupta, C.-J. Wu, X. Wang, M. Naumov, B. Reagen, D. Brooks, B. Cotel, K. Hazelwood, M. Hempstead, B. Jia, H.-H. S. Lee, A. Malevich, D. Mudigere, M. Smelyanskiy, L. Xiong, and X. Zhang, "The Architectural Implications of Facebook's DNN-based Personalized Recommendation," in *Proceedings of the International Symposium on High-Performance Computer Architecture (HPCA)*, 2020.
- [21] K. Hazelwood, S. Bird, D. Brooks, S. Chintala, U. Diril, D. Dzhulgakov, M. Fawzy, B. Jia, Y. Jia, A. Kalro, J. Law, K. Lee, J. Lu, P. Noordhuis, M. Smelyanskiy, L. Xiong, and X. Wang, "Applied Machine Learning at Facebook: A Datacenter Infrastructure Perspective," in *Proceedings of the International Symposium on High-Performance Computer Architecture (HPCA)*, 2018.
- [22] S. Hsia, U. Gupta, B. Acun, N. Ardalani, P. Zhong, G.-Y. Wei, D. Brooks, and C.-J. Wu, "MP-Rec: Hardware-Software Co-design to Enable Multi-Path Recommendation," in *Proceedings of the International Conference on Architectural Support for Programming Languages and Operating Systems (ASPLOS)*, 2023.
- [23] R. Jain, S. Cheng, V. Kalagi, V. Sanghavi, S. Kaul, M. Arunachalam, K. Maeng, A. Jog, A. Sivasubramaniam, M. T. Kandemir, and C. R. Das, "Optimizing CPU Performance for Recommendation Systems At-Scale," in *Proceedings of the International Symposium on Computer Architecture (ISCA)*, 2023.
- [24] N. Jouppi, G. Kurian, S. Li, P. Ma, R. Nagarajan, L. Nai, N. Patil, S. Subramanian, A. Swing, B. Towles, C. Young, X. Zhou, Z. Zhou, and D. A. Patterson, "TPU v4: An Optically Reconfigurable Supercomputer for Machine Learning with Hardware Support for Embeddings," in *Proceedings of the International Symposium on Computer Architecture (ISCA)*, 2023.
- [25] H. Kal, S. Lee, G. Ko, and W. W. Ro, "SPACE: Locality-Aware Processing in Heterogeneous Memory for Personalized Recommendations," in *Proceedings of the International Symposium on Computer Architecture (ISCA)*, 2021.
- [26] G. Kaur and M. M. Fuad, "An Evaluation of Protocol Buffer," in *Proceedings of the IEEE Southeastcon*, 2010.
- [27] L. Ke, U. Gupta, B. Y. Cho, D. Brooks, V. Chandra, U. Diril, A. Firoozshahian, K. Hazelwood, B. Jia, H.-H. S. Lee, M. Li, B. Maher, D. Mudigere, M. Naumov, M. Schatz, M. Smelyanskiy, X. Wang, B. Reagen, C.-J. Wu, M. Hempstead, and X. Zhang, "RecNMP: Accelerating Personalized Recommendation with Near-Memory Processing," in *Proceedings of the International Symposium on Computer Architecture (ISCA)*, 2020.
- [28] L. Ke, U. Gupta, M. Hempstead, C.-J. Wu, H.-H. S. Lee, and X. Zhang, "Hercules: Heterogeneity-Aware Inference Serving for At-Scale Personalized Recommendation," in *Proceedings of the International Symposium on High-Performance Computer Architecture (HPCA)*, 2022.
- [29] L. Ke, X. Zhang, B. Lee, G. E. Suh, and H.-H. S. Lee, "DisaggRec: Architecting Disaggregated Systems for Large-Scale Personalized Recommendation," *arXiv preprint arXiv:2212.00939*, 2022.
- [30] B. Kim, J. Park, E. Lee, M. Rhu, and J. H. Ahn, "TRIM: Tensor Reduction in Memory," *IEEE Computer Architecture Letters*, 2020.
- [31] Kubernetes, "Horizontal Pod Autoscaling," <https://kubernetes.io/docs/tasks/run-application/horizontal-pod-autoscale/>, 2023.
- [32] Kubernetes, "Kubernetes: Production-Grade Container Orchestration," <https://kubernetes.io/>, 2023.
- [33] D. H. Kurniawan, R. Wang, K. S. Zulkifli, F. A. Wiranata, J. Bent, Y. Vigfusson, and H. S. Gunawi, "EVStore: Storage and Caching Capabilities for Scaling Embedding Tables in Deep Recommendation Systems," in *Proceedings of the International Conference on Architectural Support for Programming Languages and Operating Systems (ASPLOS)*, 2023.
- [34] Y. Kwon, Y. Lee, and M. Rhu, "TensorDIMM: A Practical Near-Memory Processing Architecture for Embeddings and Tensor Operations in Deep Learning," in *Proceedings of the International Symposium on Microarchitecture (MICRO)*, 2019.
- [35] Y. Kwon, Y. Lee, and M. Rhu, "Tensor Casting: Co-Designing Algorithm-Architecture for Personalized Recommendation Training," in *Proceedings of the International Symposium on High-Performance Computer Architecture (HPCA)*, 2021.
- [36] Y. Kwon and M. Rhu, "Training Personalized Recommendation Systems from (GPU) scratch: Look Forward Not Backwards," in *Proceedings of the International Symposium on Computer Architecture (ISCA)*, 2022.
- [37] Y. Lee, S. H. Seo, H. Choi, H. U. Sul, S. Kim, J. W. Lee, and T. J. Ham, "MERIC: Efficient Embedding Reduction on Commodity Hardware via Sub-Query Memoization," in *Proceedings of the International Conference on Architectural Support for Programming Languages and Operating Systems (ASPLOS)*, 2021.
- [38] H. Liu, Q. Gao, J. Li, X. Liao, H. Xiong, G. Chen, W. Wang, G. Yang, Z. Zha, D. Dong, D. Dou, and H. Xiong, "JIZHI: A Fast and Cost-Effective Model-As-A-Service System for Web-Scale Online Inference at Baidu," in *Proceedings of the ACM SIGKDD International Conference on Knowledge Discovery & Data Mining*, 2021.
- [39] M. Lui, Y. Yetim, Ö. Özkan, Z. Zhao, S.-Y. Tsai, C.-J. Wu, and M. Hempstead, "Understanding Capacity-Driven Scale-Out Neural Recommendation Inference," in *Proceedings of the IEEE International Symposium on Performance Analysis of Systems and Software (ISPASS)*, 2021.
- [40] Meta, "Deep Learning Recommendation Model for Personalization and Recommendation Systems," <https://github.com/facebookresearch/dlrm>, 2023.

- [41] X. Miao, H. Zhang, Y. Shi, X. Nie, Z. Yang, Y. Tao, and B. Cui, "HET: Scaling Out Huge Embedding Model Training via Cache-Enabled Distributed Framework," *arXiv preprint arXiv:2112.07221*, 2021.
- [42] D. Mudigere, Y. Hao, J. Huang, Z. Jia, A. Tulloch, S. Sridharan, X. Liu, M. Ozdal, J. Nie, J. Park, L. Luo, J. A. Yang, L. Gao, D. Ivchenko, A. Basant, Y. Hu, J. Yang, E. K. Ardestani, X. Wang, R. Komuravelli, C.-H. Chu, S. Yilmaz, H. Li, J. Qian, Z. Feng, Y. Ma, J. Yang, E. Wen, H. Li, L. Yang, C. Sun, W. Zhao, D. Melts, K. Dhulipala, K. Kishore, T. Graf, A. Eisenman, K. K. Matam, A. Gangidi, G. J. Chen, M. Krishnan, A. Nayak, K. Nair, B. Muthiah, M. khorashadi, P. Bhattacharya, P. Lapukhov, M. Naumov, A. Mathews, L. Qiao, M. Smelyanskiy, B. Jia, and V. Rao, "Software-Hardware Co-Design for Fast and Scalable Training of Deep Learning Recommendation Models," in *Proceedings of the International Symposium on Computer Architecture (ISCA)*, 2022.
- [43] M. Naumov, D. Mudigere, H.-J. M. Shi, J. Huang, N. Sundaraman, J. Park, X. Wang, U. Gupta, C.-J. Wu, A. G. Azzolini, D. Dzhulgakov, A. Malleevich, I. Cherniavskii, Y. Lu, R. Krishnamoorthi, A. Yu, V. Kondratenko, S. Pereira, X. Chen, W. Chen, V. Rao, B. Jia, L. Xiong, and M. Smelyanskiy, "Deep Learning Recommendation Model for Personalization and Recommendation Systems," *arXiv preprint arXiv:1906.00091*, 2019.
- [44] S. Newman, *Building Microservices*. "O'Reilly Media, Inc.", 2021.
- [45] NVIDIA, "Accelerating Recommendation System Inference Performance with TensorRT," <https://developer.nvidia.com/blog/accelerating-recommendation-system-inference-performance-with-tensorrt/>, 2018.
- [46] NVIDIA, "NVIDIA Merlin: Recommender System Framework," <https://developer.nvidia.com/merlin>, 2023.
- [47] NVIDIA, "NVIDIA T4," <https://www.nvidia.com/en-us/data-center/tesla-t4/>, 2023.
- [48] C. Olston, N. Fiedel, K. Gorovoy, J. Harmsen, L. Lao, F. Li, V. Rajashekhar, S. Ramesh, and J. Soyke, "TensorFlow-Serving: Flexible, High-Performance ML Serving," *arXiv preprint arXiv:1712.06139*, 2017.
- [49] J. Park, M. Naumov, P. Basu, S. Deng, A. Kalaiah, D. Khudia, J. Law, P. Malani, A. Malevich, S. Nadathur, J. Pino, M. Schatz, A. Sidorov, V. Sivakumar, A. Tulloch, X. Wang, Y. Wu, H. Yuen, U. Diril, D. Dzhulgakov, K. Hazelwood, B. Jia, Y. Jia, L. Qiao, V. Rao, N. Rotem, S. Yoo, and M. Smelyanskiy, "Deep Learning Inference in Facebook Data Centers: Characterization, Performance Optimizations and Hardware Implications," *arXiv preprint arXiv:1811.09886*, 2018.
- [50] Prometheus, "Prometheus: From Metrics to Insight," <https://prometheus.io/>, 2023.
- [51] PyTorch, "Torch Serve," <https://pytorch.org/serve/>, 2023.
- [52] G. Sethi, B. Acun, N. Agarwal, C. Kozyrakis, C. Trippel, and C.-J. Wu, "RecShard: Statistical Feature-Based Memory Optimization for Industry-Scale Neural Recommendation," in *Proceedings of the International Conference on Architectural Support for Programming Languages and Operating Systems (ASPLOS)*, 2022.
- [53] X. Song, Y. Zhang, R. Chen, and H. Chen, "UGACHE: A Unified GPU Cache for Embedding-based Deep Learning," in *Proceedings of the ACM Symposium on Operating System Principles (SOSP)*, 2023.
- [54] R. Srinivasan, "RPC: Remote Procedure Call Protocol Specification Version 2," Tech. Rep., 1995.
- [55] X. Sun, H. Wan, Q. Li, C.-L. Yang, T.-W. Kuo, and C. J. Xue, "RM-SSD: In-Storage Computing for Large-Scale Recommendation Inference," in *Proceedings of the International Symposium on High-Performance Computer Architecture (HPCA)*, 2022.
- [56] Z. Wang, Y. Wei, M. Lee, M. Langer, F. Yu, J. Liu, S. Liu, D. G. Abel, X. Guo, J. Dong *et al.*, "Merlin HugeCTR: GPU-Accelerated Recommender System Training and Inference," in *Proceedings of the ACM Conference on Recommender Systems (RecSys)*, 2022.
- [57] M. Wilkening, U. Gupta, S. Hsia, C. Trippel, C.-J. Wu, D. Brooks, and G.-Y. Wei, "RecSSD: Near Data Processing for Solid State Drive Based Recommendation Inference," in *Proceedings of the International Conference on Architectural Support for Programming Languages and Operating Systems (ASPLOS)*, 2021.
- [58] M. Xie, Y. Lu, J. Lin, Q. Wang, J. Gao, K. Ren, and J. Shu, "Fleche: An Efficient GPU Embedding Cache for Personalized Recommendations," in *Proceedings of the European Conference on Computer Systems (EuroSys)*, 2022.
- [59] C. Yin, B. Acun, C.-J. Wu, and X. Liu, "TT-Rec: Tensor Train Compression for Deep Learning Recommendation Models," 2021.
- [60] W. Zhao, J. Zhang, D. Xie, Y. Qian, R. Jia, and P. Li, "AIBox: CTR Prediction Model Training on A Single Node," in *Proceedings of the ACM International Conference on Information and Knowledge Management*, 2019.